Molecular Cell
Article

Modular Assembly of RWD Domains on the Mis12 Complex Underlies Outer Kinetochore Organization

Arsen Petrovic,[1,6] Shyamal Mosalaganti,[2,6] Jenny Keller,[1,6] Marta Mattiuzzo,[1] Katharina Overlack,[1] Veronica Krenn,[1] Anna De Antoni,[3] Sabine Wohlgemuth,[1] Valentina Cecatiello,[4] Sebastiano Pasqualato,[4] Stefan Raunser,[2] and Andrea Musacchio[1,5,*]
[1]Department of Mechanistic Cell Biology
[2]Department of Physical Biochemistry
Max Planck Institute of Molecular Physiology, Otto-Hahn-Straße 11, 44227 Dortmund, Germany
[3]Chromosome Segregation Group, Department of Experimental Oncology
[4]Crystallography Unit, Department of Experimental Oncology
European Institute of Oncology, Via Adamello 16, Milan, Italy
[5]Centre for Medical Biotechnology, Faculty of Biology, University Duisburg-Essen, Universitätsstrasse, 45141 Essen, Germany
[6]These authors contributed equally to this work
*Correspondence: andrea.musacchio@mpi-dortmund.mpg.de
http://dx.doi.org/10.1016/j.molcel.2014.01.019

SUMMARY

Faithful chromosome segregation is mandatory for cell and organismal viability. Kinetochores, large protein assemblies embedded in centromeric chromatin, establish a mechanical link between chromosomes and spindle microtubules. The KMN network, a conserved 10-subunit kinetochore complex, harbors the microtubule-binding interface. RWD domains in the KMN subunits Spc24 and Spc25 mediate kinetochore targeting of the microtubule-binding subunits by interacting with the Mis12 complex, a KMN subcomplex that tethers directly onto the underlying chromatin layer. Here, we show that Knl1, a KMN subunit involved in mitotic checkpoint signaling, also contains RWD domains that bind the Mis12 complex and that mediate kinetochore targeting of Knl1. By reporting the first 3D electron microscopy structure of the KMN network, we provide a comprehensive framework to interpret how interactions of RWD-containing proteins with the Mis12 complex shape KMN network topology. Our observations unveil a regular pattern in the construction of the outer kinetochore.

INTRODUCTION

The molecular events that control the seamless segregation of chromosomes during mitosis and meiosis are among the most exciting examples of self-organization in living matter. The command of operation is in the hands of kinetochores, complex macromolecular structures tethered on chromosomes (Santaguida and Musacchio, 2009; Westermann and Schleiffer, 2013). The so-called inner kinetochore, which contains at least 15 constitutive centromere-associated network (CCAN) subunits, interacts with specialized chromatin in the centromere region of chromosomes. The outer kinetochore, which assembles on the inner kinetochore layer prior to mitosis, creates sturdy, load-bearing interfaces for binding to spindle microtubules.

Besides being responsible for microtubule binding and stabilization, the outer kinetochore controls the spindle assembly checkpoint (SAC, also known as mitotic checkpoint), a feedback mechanism that targets the cell-cycle machinery to prevent premature exit from mitosis in the presence of tensionless kinetochores (Foley and Kapoor, 2013; Lara-Gonzalez et al., 2012). Thus, the outer kinetochore plays crucial mechanical and regulatory roles in chromosome segregation: it attaches to the spindle and concomitantly synchronizes the cell-cycle machinery with the state of attachment through SAC signaling. Perturbations of this signaling pathways lead to defects in chromosome segregation and to the creation of aneuploid progeny (Foley and Kapoor, 2013; Lara-Gonzalez et al., 2012).

The KMN network, a 10-subunit assembly with an approximate molecular mass of 590 kDa in humans, is the core of the outer kinetochore (Cheeseman and Desai, 2008; Foley and Kapoor, 2013). The KMN network is assembled from three distinct subcomplexes (Figure 1A). The Knl1 subcomplex (herewith identified as Knl1-C) comprises the subunits Knl1 (also known as Spc105, Spc7, CASC5, AF15q14, and Blinkin. Alternative names for KMN subunits are discussed in the legend to Figure 1A) and Zwint. The Mis12 subcomplex (herewith Mis12-C) comprises the subunits Dsn1, Mis12, Nnf1, and Nsl1. The Ndc80 subcomplex (Ndc80-C) comprises Ndc80 (also known as Hec1), Nuf2, Spc24, and Spc25. Seven to twenty KMN network complexes may participate in the binding of a single microtubule (Joglekar et al., 2009, 2006; Johnston et al., 2010).

The KMN subcomplexes have specialized functions. Mis12-C interacts with the CCAN subunit CENP-C and is the crucial point of tethering of the outer kinetochore on the inner kinetochore (Przewloka et al., 2011; Screpanti et al., 2011). Once associated with kinetochores, Mis12-C provides a binding platform for Ndc80-C and Knl1-C (Hornung et al., 2011; Kiyomitsu et al., 2010; Kline et al., 2006; Maskell et al., 2010; Petrovic et al., 2010; Wan et al., 2009) (Figure 1B). Ndc80-C forms an additional stabilizing interaction with CENP-T (Bock et al., 2012; Gascoigne et al., 2011; Hori et al., 2008; Schleiffer et al., 2012).

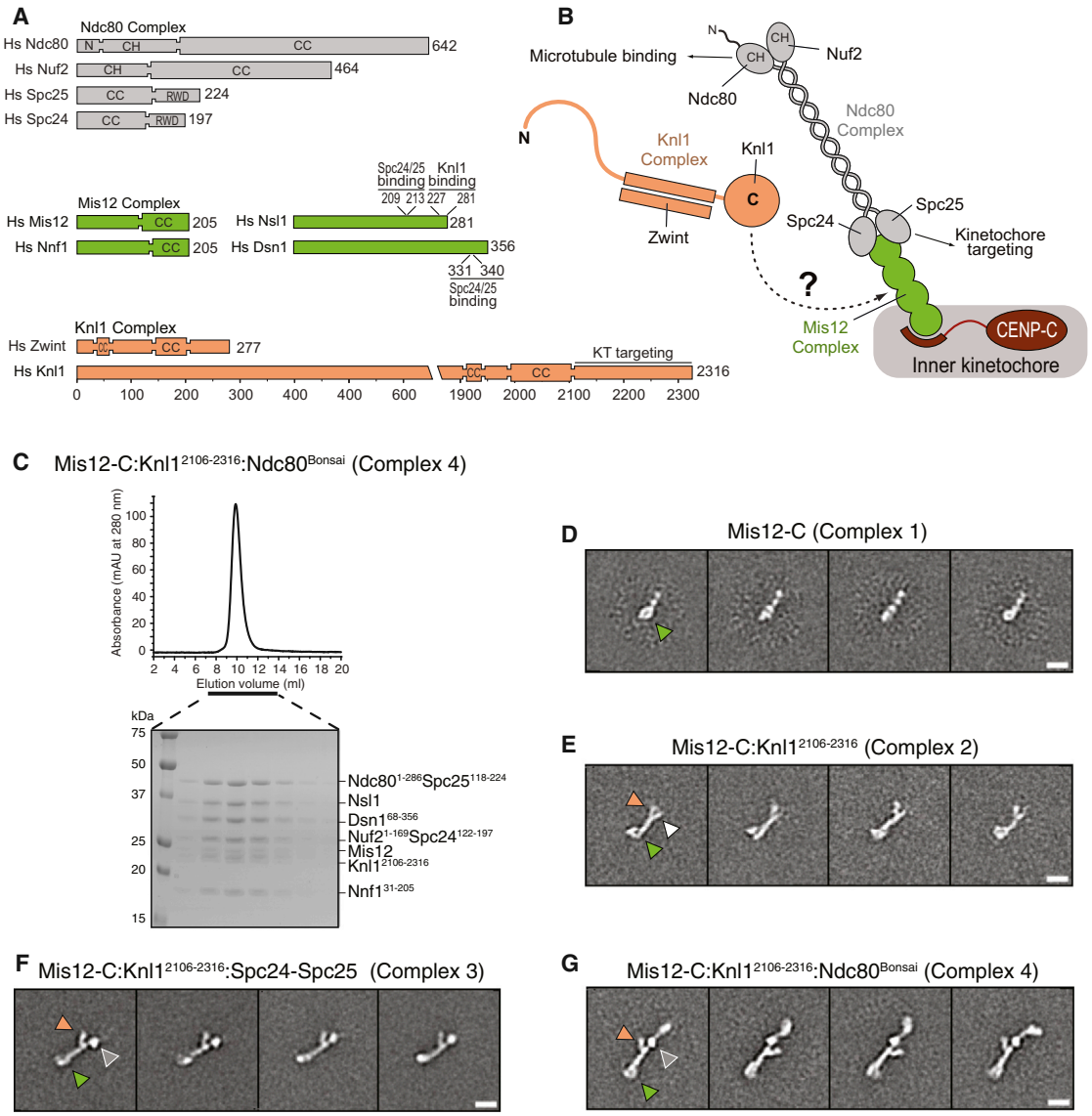

Figure 1. Structural Organization of the KMN Network and Its Interaction with Knl1

(A) Schematic view of the organization of the KMN network. There are Calponin homology (CH) domains at the N-terminal ends of the Ndc80 subunit (also known as Hec1). In Ndc80, an N-terminal extension (N) precedes the CH. Coiled coils (CC) mediate intersubunit interactions. The structures of subunits of Mis12-C are unknown. HsNnf1 is also known as PMF1, HsDsn1 is also known as C20orf72, and HsNsl1 is also known as DC31. Zwint is also identified as Zwint-1. The position of known Ndc80- and Knl1-binding regions is indicated. Knl1 contains motifs for interaction with checkpoint components and the PP1 phosphatase (not shown in this scheme). The position of the C-terminal kinetochore-localization domain is indicated. Zwint binds Knl1 between residues ~1,900 and the C terminus (Hodson et al., 2011; Kiyomitsu et al., 2011).

(B) Summary of KMN structural organization. Globular domains at the two ends of the Ndc80-C rod mediate interactions with microtubules and kinetochores, respectively. A direct interaction of CENP-C with Mis12-C tethers Mis12-C at kinetochores. The question mark indicates that the position at which Knl1-C docks on Mis12-C is unknown.

(C) Size-exclusion chromatography profile of Complex 4 (Mis12-C:Knl1$^{2106-2311}$:Ndc80-C^{Bonsai}).

(D) Representative class averages of Mis12-C. In this and subsequent panels, the green arrowhead marks the "thick" end of Mis12-C. Scale bar, 10 nm in (D)–(G).

(E) Representative class averages of Mis12-C:Knl1$^{2106-2311}$. The orange arrowhead marks a new feature, not present in Complex 1, which likely represents the Knl1 C-terminal domain. The white arrow marks features of Mis12-C, extending beyond the Knl1 binding site, that merge with Ndc80 in those complexes in which the latter is also present.

(F) Representative class averages of Mis12-C:Knl1$^{2106-2311}$:Spc24-Spc25. The gray arrowhead marks the position of the Spc24 and Spc25 subunits.

(G) Representative class averages of Mis12-C:Knl1$^{2106-2311}$:Ndc80-C^{Bonsai}. The gray arrowhead marks Ndc80-C^{Bonsai}.

Ndc80-C, rich in coiled coil and highly elongated (~55 nm), contains two small globular regions at either end of the rod (Cheeseman et al., 2006; Ciferri et al., 2005, 2008; DeLuca et al., 2006; Wang et al., 2008; Wei et al., 2005, 2006, 2007). One end contains the calponin-homology (CH) domains of the Ndc80 and Nuf2 subunits, which have been implicated in microtubule binding. The other end contains the Spc24 and Spc25 subunits, which target Ndc80-C to kinetochores (Cheeseman et al., 2006; Ciferri et al., 2008; DeLuca et al., 2006) (Figures 1A and 1B). The Spc24 and Spc25 subunits are structurally related and consist of N-terminal coiled-coil motifs followed by C-terminal RING finger, WD repeat, DEAD-like helicases (RWD) domains (Ciferri et al., 2008; Malvezzi et al., 2013; Nishino et al., 2013; Wei et al., 2006) (Figure 1A). The RWD domains mediate kinetochore recruitment through interactions with at least two distinct sequence motifs on the Nsl1 and Dsn1 subunits of MIS12-C (Malvezzi et al., 2013; Petrovic et al., 2010) (Figure 1A).

Knl1-C is directly responsible for the recruitment of checkpoint components, including Bub1, BubR1, and Bub3 (Kiyomitsu et al., 2007; Krenn et al., 2012; London et al., 2012; Pagliuca et al., 2009; Primorac et al., 2013; Shepperd et al., 2012; Yamagishi et al., 2012). It has also been implicated in microtubule binding and in recruiting the PP1 phosphatase, whose activity is required for chromosome alignment and for SAC silencing (Espeut et al., 2012; Liu et al., 2010; Meadows et al., 2011; Rosenberg et al., 2011). Kinetochore targeting of Knl1-C requires the C-terminal region of Knl1 (Kiyomitsu et al., 2007, 2010, 2011; Petrovic et al., 2010). In vitro, the latter was shown to bind to the C-terminal segment of the Mis12-C subunit Nsl1 (residues 227–281), with residues 259–281 being necessary for the interaction (Petrovic et al., 2010) (Figure 1A).

The C-terminal region of Knl1 is the only segment of this 2,316-residue protein predicted to have a globular fold. However, its structure is uncharacterized, and so is the mechanism of its interaction with Nsl1. Here we report the crystal structure of the C-terminal domain of Knl1 and report the surprising finding that it contains a tandem RWD arrangement. We also reveal the structure of the Nsl1-Knl1 complex, and identify the position of the Knl1 C-terminal domain and of other crucial features of the KMN network in the first three-dimensional (3D) structure of the KMN network by single-particle electron microscopy (EM). We propose that specialized interactions of the Mis12 complex with RWD domains are the basis for the function of MIS12-C as an interaction hub at the kinetochore.

RESULTS

Single-Particle EM Analysis Identifies the Site of Docking of Knl1 on the KMN Network

To identify the position along Mis12-C on which Knl1 docks, we reconstituted four complexes from recombinant versions of the human KMN subunits (see Figure S1 available online; data not shown), including the isolated Mis12-C (Complex 1), the Mis12-C:Knl1$^{2106-2316}$ complex (Complex 2), the Mis12-C:Knl1$^{2106-2316}$:Spc24-Spc25 complex (Complex 3), and the Mis12-C:Knl1$^{2106-2316}$:Ndc80-C^{Bonsai} complex (Complex 4) (Figures S1 and 1C). Ndc80-C^{Bonsai} is an engineered dimeric version of the tetrameric Ndc80 complex retaining the kinetochore targeting domain of the Spc24 and Spc25 subunits, as well as the microtubule-binding domain of the Ndc80 and Nuf2 subunits, but from which a large fragment of the coiled coil in the central shaft of the complex had been removed. The structure of Ndc80-C^{Bonsai} has been determined to high resolution (Ciferri et al., 2008).

We analyzed all four complexes by single-particle negative-stain EM and calculated class averages for each of the complexes (Figures 1D–1G and S3). As shown previously (Hornung et al., 2011; Maskell et al., 2010; Petrovic et al., 2010; Screpanti et al., 2011), the Mis12 complex appeared elongated, with one end (marked by a green arrowhead in Figure 1D and in following panels) significantly thicker and structurally more complex than the other. Comparison of class averages of the isolated Mis12-C and of its complexes with the Knl1 C-terminal domain and with Ndc80-C constructs unequivocally identified the Knl1$^{2106-2316}$ domain as a density emerging laterally from the long axis of the Mis12-C, and diverging from it at an approximately 60° angle (shown by orange arrowheads in Figures 1D–1G; see also Figure S3).

The point of contact of the Knl1 C-terminal domain on Mis12-C flanks the thin end of Mis12-C (see averages of Complex 2). The segment of Mis12-C that extends beyond the point of contact with Knl1 and toward the Mis12-C's proximal end in Complex 2 (indicated with a white arrowhead) appears to contain binding sites for Ndc80-C (indicated by gray arrowheads in Complex 3 and 4), because it becomes integrated into the densities corresponding to Spc24-Spc25 or Ndc80-C^{Bonsai} in Complexes 3 and 4. Thus, the end of Mis12-C proximal to the Knl1 C-terminal domain binding site also contains the Ndc80-interacting regions of Nsl1 and Dsn1. Previously, the interaction sites for Ndc80-C have been mapped to the C-terminal region of Dsn1 (Malvezzi et al., 2013) and to a motif with sequence Pro-Val-Ile-His-Leu at residues 209–213 of Nsl1 (Kiyomitsu et al., 2010; Petrovic et al., 2010), approximately 50–60 residues upstream from the Knl1-binding motif of Nsl1 (Petrovic et al., 2010) (Figure 1A).

Structural Analysis of the Knl1 C-Terminal Domain

To gain insight into the structure of the Knl1 C-terminal domain, we determined the crystal structure of a construct encompassing residues 2,106–2,311 of human Knl1 (Knl1$^{2106-2311}$) by the multiple isomorphous replacement (MIR) method to a maximal resolution of 2.5 Å and with good stereochemical parameters (Table 1). This analysis revealed that Knl1$^{2106-2311}$ consists of a tandem arrangement of two RWD domains (RWD-N and RWD-C, encompassing residues 2,109–2,209 and 2,210–2,311, respectively), connected by a continuous ~32-residue helix that is shared by the two domains (Figures 2A and 2B). Overall, the tandem arrangement of RWD domains gives rise to a rather elongated structure with a long axis of approximately 7 nm and short axes of approximately 2 and 2.5 nm. The fold of RWD domains is classified within a superfamily of Ubiquitin (Ub)-conjugating (E2) enzymes (UBC) (Doerks et al., 2002). However, RWD domains lack the catalytic machinery required for covalent Ub binding and substrate transfer, and are usually involved in protein-protein interactions (Burroughs et al., 2008).

Table 1. Data Collection, Phasing, and Refinement Statistics

Data Collection	$KNL1^{2106-2311}$					$KNL1^{2091-2311}$: $Nsl1^{256-281}$
	Native	K2PtBr4 10 mM, Overnight	NaBr 500 mM, 25″			SeMet
Beamline	ESRF, ID14-1	ESRF, ID14-4	ESRF, ID14-4			SLS, PXIII
Spacegroup	$P3_121$	$P3_121$	$P3_121$			$P2_12_12_1$
Unit cell parameters: a (Å)	74.855	74.863	74.666			60.710
b (Å)	74.855	74.863	74.666			71.630
c (Å)	88.756	88.787	88.293			177.210
α (°)	90	90	90			90
β (°)	90	90	90			90
γ (°)	120	120	120			90
		Peak	Peak	Inflection Point	High-Energy Remote	Peak
Wavelength (Å)	0.933	1.072	0.9195	0.9200	0.9160	1.0006
Resolution limits (Å)	50–2.50 (2.59–2.50)[a]	50–2.40 (2.49–2.40)[a]	50–2.50 (2.59–2.50)[a]	50–2.50 (2.59–2.50)[a]	50–2.50 (2.59–2.50)[a]	46–2.80 (2.87–2.80)[a]
Reflections	10,352	11,860	10,248	10,334	10,281	36,465
Completeness (%)	99.8 (100.0)[a]	99.8 (99.5)[a]	100.0 (100.0)[a]	100.0 (100.0)[a]	99.9 (100.0)[a]	99.5 (99.6)[a]
R_{symm}[c] (%)	4.4 (33.2)[a]	7.7 (56.6)[a]	7.1 (60.3)[a]	7.9 (>100)[a]	6.0 (61.8)[a]	8.7 (55.8)[a]
R_{pim}[d] (%)	1.4 (14.0)[a]	1.1 (10.8)[a]	1.0 (11.5)[a]	1.7 (28.9)[a]	1.1 (16.5)[a]	5.0 (31.2)[a]
I/σI	16.2 (2.3)[a]	50.1 (10.9)[a]	68.2 (10.3)[a]	44.3 (3.7)[a]	44.3 (3.7)[a]	14.1 (2.7)[a]
Redundancy	10.7 (9.3)[a]	42.3 (38.4)[a]	42.9 (43.2)[a]	21.0 (18.1)[a]	21.5 (22.0)[a]	3.91 (3.9)[a]
Phasing and Automatic Model Building with Auto-Rickshaw						
SHELXD CC/CC (weak)		42.55/26.37		26.22/11.10		
Sites found by SHELXD/refined sites		1/1 Pt		2/9 Br		
Number of residues built automatically (210 total) (SHELXE, RESOLVE and ARP/wARP)		200		199		
Structure Refinement						
Resolution[b] (Å)	32.4–2.50 (2.75–2.50)[b]	19.4–2.40 (2.59–2.40)[b]	36.5–2.50 (2.75–2.50)[b]			20.0–2.80 (2.87–2.80)[b]
Reflections for R_{cryst} / for R_{free}	9,830/498	10,898/707	9,725/494			18,673/983
R_{cryst}[e] (%)	19.3 (22.4)[b]	19.0 (24.2)[b]	19.8 (24.3)[b]			20.1 (31.6)[b]
R_{free}[e] (%)	24.2 (28.9)[b]	23.5 (31.3)[b]	24.5 (32.5)[b]			25.9 (41.7)[b]
Number of protein atoms /number of water atoms	1,684 / 101	1,713 / 106	1,691 / 95			3,669/47
Average B factor protein atoms ($Å^2$)	52.7	55.0	53.8			59.5
Rmsd bond lengths (Å)	0.007	0.016	0.009			0.016
Rmsd bond angles (°)	1.03	1.13	0.84			1.867
Ramachandran Plot (%)						
Favored	95.5	95.5	97.0			94.2
Allowed	4.5	4.5	2.5			5.8
Outliers	0	0	0.5			0

[a]Values in parentheses correspond to highest-resolution shell.
[b]Values in parentheses correspond to highest-resolution shell used in refinement.
[c]$R_{symm} = \frac{\sum_{hkl}\sum_j |I_{hkl,j} - \langle I_{hkl}\rangle|}{\sum_{hkl}\sum_j I_{hkl,j}}$.
[d]$R_{pim} = \frac{\sum_{hkl}\sqrt{\frac{1}{n-1}}\sum_{j=1}^{n} |I_{hkl} - \langle I_{hkl}\rangle|}{\sum_{hkl}\sum_j I_{hkl,j}}$; R_{pim} calculated as discussed in Experimental Procedures.
[e]R_{cryst} and $R_{free} = \frac{\sum |F_{obs} - F_{calc}|}{\sum F_{obs}}$; R_{free} calculated for a 5% subset of reflections not used in the refinement.

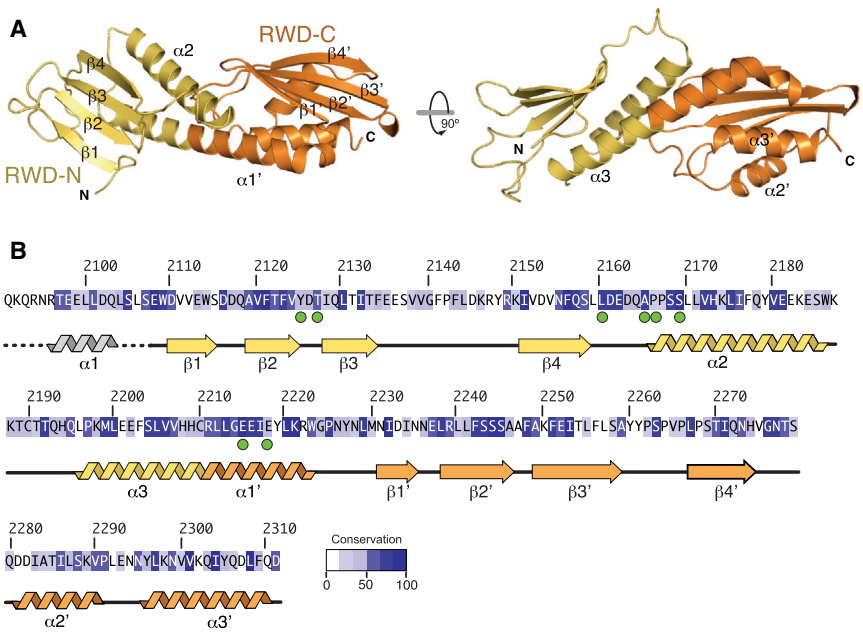

Figure 2. Crystal Structure of the Knl1 C-Terminal Domain

(A) The cartoon model of the crystal structure of Knl1$^{2106-2311}$ shows that it consists of a tandem arrangement of RWD domains, RWD-N and RWD-C, colored yellow and orange, respectively. All protein models were obtained with Pymol (PyMOL Molecular Graphics System, Version 1.5.0.4 Schrödinger, LLC.) and further imported in Adobe Illustrator.

(B) Amino acid sequence of the C-terminal region of human Knl1 with secondary structure. The N-terminal α1 helix is only observed in one of the two molecules in the asymmetric unit of the Knl1-Nsl1 complex and is marked on the alignment for completeness. Residues are colored according to the degree of conservation measured on the basis of the alignment shown in Figure S4. Green circles indicate residues at the interface with the Nsl1 peptide (based on crystal structure depicted in Figure 4D).

Prior to our discovery of RWD domains in the C-terminal kinetochore-targeting region of Knl1, RWD domains had been identified in several other kinetochore proteins, including Spc24, Spc25, Mad1, the monopolin subunit Csm1, and the inner kinetochore subunits Mcm21 and Ctf19 (orthologous to human CENP-P and CENP-O, respectively) (Figure 3A). Spc24, Spc25, Mad1, and Csm1 contain a single RWD domain (Ciferri et al., 2008; Corbett et al., 2010; Kim et al., 2012; Wei et al., 2006). Conversely, Mcm21 and Ctf19 contain a tandem arrangement of RWD domains that is very similar to the one observed in Knl1 (Schmitzberger and Harrison, 2012) (Figure S5).

Irrespective of whether they contain single or tandem RWD domains, all these kinetochore proteins display a similar topology, in which a segment of variable length with high propensity to form a coiled-coil precedes the RWD domain(s). We observed the same arrangement in Knl1 (Figure 1A), suggesting that all these proteins might have originated from a common ancestor. In agreement with this hypothesis, RWD domains are present in many additional proteins, but generally they are not located near the host protein's C terminus and are not preceded by coiled-coil segments (see entry PF05773 in the PFAM database at http://pfam.sanger.ac.uk/).

Oligomerization of Knl1 and Its Determinants

As shown in Figure 3A, all known RWD-containing kinetochore proteins, irrespective of whether they contain one or two RWD domains, form homo- or heterodimers of similar topology. Such dimeric arrangements are held together through contributions from the parallel pairing of the helical segments preceding the RWD domains, as well as by additional interactions at the interface between RWD domains. In crystals of the Knl1$^{2106-2311}$ or Knl1$^{2091-2311}$ bound to Nsl1, no obvious dimeric arrangement of Knl1 was evident. Furthermore, these constructs eluted as expected for monomeric species in size-exclusion chromatography (SEC) experiments (data not shown). We therefore analyzed the hydrodynamic properties of a recombinant version of Knl1$^{2000-2311}$, a construct containing a longer fragment of the predicted coiled-coil region that precedes the RWD domains. SEC and static light scattering experiments indicated that over 90% of Knl1$^{2000-2311}$ was monomeric (Figure 3B), with a predicted molecular weight of ~38.6 kDa, in good agreement with the theoretical molecular weight of ~36.9 kDa. Only less than 10% of the sample ran in a separate peak that was compatible with formation of a dimer. Thus, a fragment of Knl1 containing approximately 100 residues of a predicted coiled-coil segment followed by the tandem RWD domains is unable to form stable dimers in solution.

Due to poor solubility of the recombinant material, we could not include in our analysis of Knl1 dimerization additional constructs bearing segments extending further toward the Knl1 N terminus. We therefore generated stable inducible HeLa cell lines expressing GFP fusions of fragments of Knl1 that were not accessible to the analysis in vitro (Figure 3C). GFP-Knl1$^{1834-2316}$ encompasses the entire predicted coiled-coil region of Knl1 and additional N-terminal sequences. This construct, as well as the other ones discussed in the remains of this paragraph, correctly targeted to kinetochores (data not shown). Immunoprecipitation experiments from lysates expressing Knl1$^{1834-2316}$-GFP identified the KMN subunits Ndc80 and Mis12, as expected based on the presence of the RWD kinetochore-targeting domains in the expressed Knl1 segment (Figure 3C). Knl1$^{1834-2316}$-GFP also pulled down Zwint. GFP-Knl1$^{2107-2316}$, which lacks the predicted coiled-coil segment, also interacted with Ndc80 and Mis12 but was unable to interact with Zwint, indicating that the coiled-coil region of Knl1 is required for this interaction (Kiyomitsu et al., 2011) (Figure 3C). No endogenous Knl1 was detected in the Knl1$^{1834-2316}$-GFP or

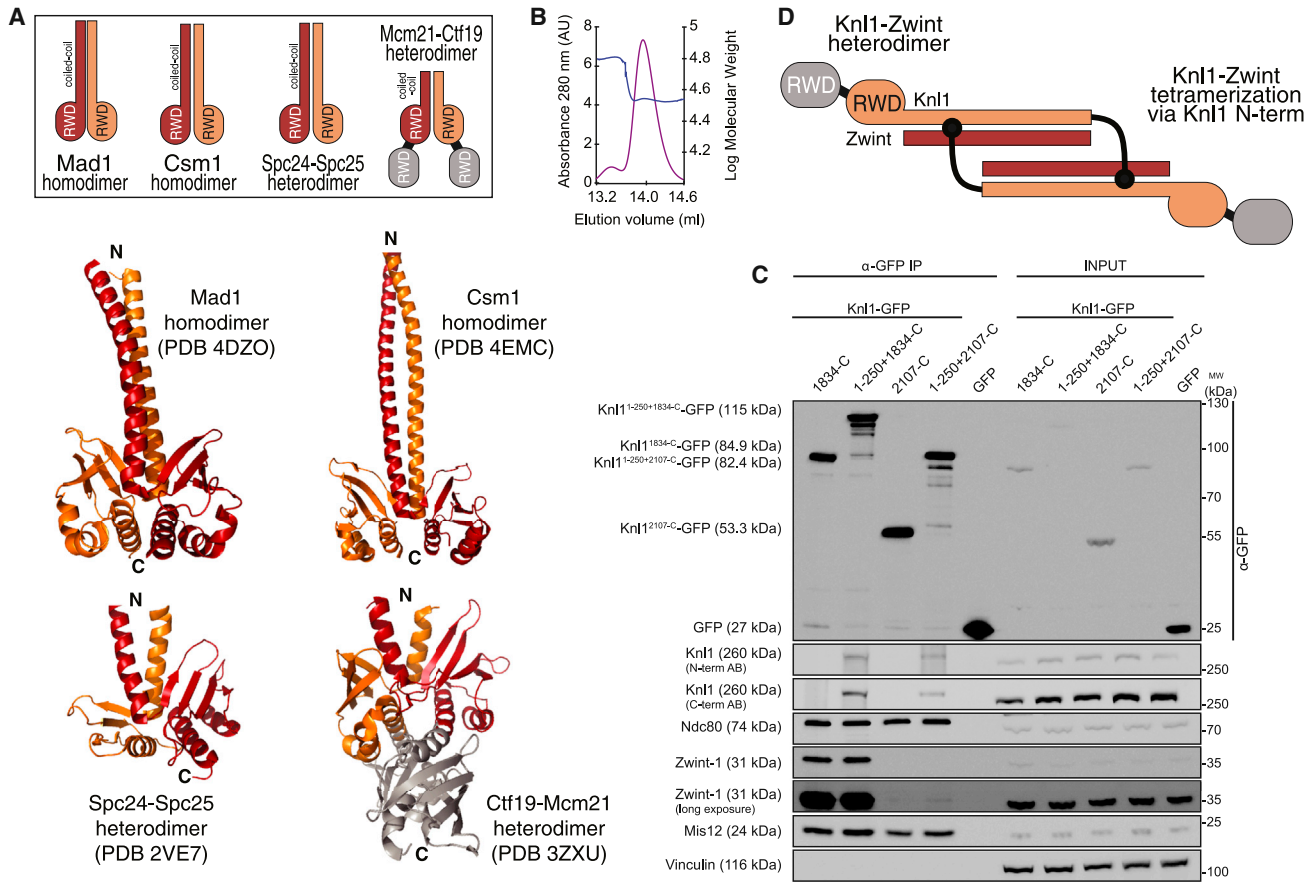

Figure 3. Dimerization of Knl1

(A) Schematic view and cartoon models of RWD-containing kinetochore subunits or complexes. To emphasize the dimeric arrangement, the polypeptide chains in each of the indicated homodimers or heterodimers are shown in dark red and orange. The RWD-C of Ctf19 and Mcm21 are shown in gray. All four assemblies shown, which include all known RWD-domain-containing kinetochore proteins except Knl1, show similar topologies, with N-terminal helical segments of variable length, and C-terminal RWD domains.

(B) Static light scattering analysis of fractions eluting from a size-exclusion chromatography separation of the Knl1$^{2000-2311}$ construct.

(C) The indicated Knl-GFP constructs were expressed in HeLa Flp-In T-REx cells from stably integrated transgenes after induction with Doxycycline. Immunoprecipitations (IP) were performed with anti-GFP antibody, and the presence of the indicated proteins was analyzed by western blotting.

(D) Interpretation of results in (C). Zwint is proposed to resemble the C-terminal region of Knl1 and to pair with Knl1 through the Knl1 helical domain, but it lacks C-terminal RWD domain(s). The N-terminal region of Knl1 (black) is shown to mediate higher-order oligomerization. The exact binding site of the N-terminal region of Knl1 is unknown.

Knl1$^{2107-2316}$-GFP precipitates, suggesting that once paired with Zwint the C-terminal region of Knl1 might be per se unable to form higher-order oligomers.

In a separate study (Krenn et al., 2014) we have shown that a chimeric protein containing the first 250 residues of Knl1 fused to residues 1,834–2,316 (Knl1$^{1-250+1834-2316}$) efficiently complements the negative effects of RNAi-based Knl1 depletion in HeLa cells on chromosome alignment and spindle checkpoint signaling. Here, we show that when expressed in HeLa cells, Knl1$^{1-250+1834-2316}$ effectively interacted with Ndc80 and Mis12. Remarkably, it also efficiently pulled down endogenous Knl1 (Figure 3C). Thus, the first 250 residues of Knl1 contain a motif that mediates, either directly or indirectly, the oligomerization of Knl1. As these experiments were carried out in nocodazole, and therefore in the absence of microtubules, this behavior is unlikely to reflect oligomerization of Knl1 on the microtubule lattice through the Knl1 microtubule-binding domain (Espeut et al., 2012). Knl1$^{1-250+1834-2316}$ interacted with endogenous Knl1 irrespective of the status of the SAC and did so also in mitotic cells in the presence of microtubules (V.K, K.O., and A.M., unpublished data).

Finally, we asked if the predicted coiled-coil region of Knl1$^{1-250+1834-2316}$ was required for its ability to pull down endogenous Knl1. Knl1$^{1-250+2107-2316}$, which lacks the predicted coiled-coil region and is unable to bind Zwint directly, retained the ability to pull down endogenous Knl1 (as well as endogenous Zwint, whose weak signal is visible in Figure 3C), albeit with slightly reduced efficiency. Thus, presence of the predicted coiled-coil region in our construct might be dispensable for Knl1 oligomerization mediated by the N-terminal region. Although the Knl1-GFP bait constructs lacking the predicted helical segment were unable to interact with Zwint, our experiments do not rule

out a role of Zwint in the precipitation of endogenous Knl1 with such Knl1-GFP baits.

Determinants of the Knl1-Nsl1 Interaction

Previously, we identified a C-terminal segment of human Nsl1 encompassing residues 258–281 ($Nsl1^{258-281}$) as being necessary for the binding of Knl1 in vitro and for Knl1 recruitment to kinetochores in human cells (Petrovic et al., 2010). The Nsl1 C-terminal motif is conserved in vertebrates (Figure 4A) and possibly also in fungi (Figure S4B). We used isothermal titration calorimetry (ITC) to test whether $Nsl1^{258-281}$ is also sufficient for a tight interaction with Knl1. Specifically, we measured the dissociation constant (K_D) of the interaction of $Knl1^{2000-2311}$ with the entire Mis12-C (the Mis12 holo-complex) or with an isolated synthetic peptide encompassing the $Nsl1^{258-281}$ sequence. $Knl1^{2000-2311}$ bound Mis12-C or $Nsl1^{258-281}$ with K_D values of 33 nM and ~250 nM, respectively (Figures 4B and 4C). The relatively small (8-fold) reduction of binding affinity when using the Nsl1 peptide instead of Mis12-C indicates that the binding of the RWD domains of Knl1 with the C-terminal tail of Nsl1 dominates the interface with Mis12-C. Additional contacts with Mis12-C, also suggested by our EM analysis in Figure 6, might account for the relatively modest increase in binding affinity when the C-terminal tail of Nsl1 is presented to Knl1 in the context of Mis12-C rather than as an isolated peptide. There was no observable difference between $Knl1^{2000-2311}$ and shorter constructs of Knl1 ($Knl1^{2091-2311}$ and $Knl1^{2106-2311}$) in binding to the Nsl1 peptide (data not shown).

Structural Analysis of the Knl1-Nsl1 Complex

Results in the previous section identified the minimal structural elements required for the high-affinity interaction between the Mis12 complex and the kinetochore-targeting domain of Knl1. To gain structural information on this interaction, we obtained crystals of a preformed complex of $Knl1^{2091-2311}$ with the $Nsl1^{258-281}$ peptide. We collected diffraction data to a resolution of 2.8 Å. The crystal structure of the Knl1-Nsl1 complex was determined by molecular replacement on a data set collected from a selenomethionine (SeMet) derivative of $Knl1^{2091-2311}$ (Table 1).

There was interpretable electron density for residues 266–274 of the Nsl1 peptide (Figure S4). The latter positions itself in a cradle surrounded by the β2-β3 loop, the β4-α2 loop, and the α1′ helix, thus engaging residues from both RWD domains, but with a more extensive involvement of RWD-N (Figure 4D). The first part of the Nsl1 peptide (residues 266–269) forms a single tight helical turn, whereas the second part (residues 270–274) is extended (Figure 4D). The side chains of $Trp269^{Nsl1}$ and $Tyr270^{Nsl1}$ are extensively involved in the packing of the Nsl1 peptide against $Knl1^{2091-2311}$, with the side chain of $Tyr270^{Nsl1}$ becoming completely buried around the side chains of $Tyr2125^{Knl1}$, $Leu2160^{Knl1}$, and $Ser2169^{Knl1}$. Furthermore, the side chain hydroxyl of $Ser2169^{Knl1}$ is hydrogen bonded to the main-chain carbonyl of $Trp269^{Nsl1}$. Additional hydrogen bonds are contributed by the side chain of $Arg267^{Nsl1}$ and by main-chain interactions between the extended region of the Nsl1 peptide and the β4-α2 loop. Knl1 residues positioned at the interface with Nsl1 are evolutionarily conserved (Figures 2B and 4E).

Superposition of the models of unbound Knl1 and Nsl1-bound Knl1 shows that the RWD-N domain of Knl1 undergoes a very significant conformational change upon binding to Nsl1 (Figure 4F). Most notably, the entire β2-strand undergoes a two-residue shift of register, resulting in the extrusion of the side chain of $Tyr2125^{Knl1}$ in the Nsl1-bound structure. $Tyr2125^{Knl1}$ is instead buried within the hydrophobic core of the unbound RWD-N of Knl1 (Figure 4F). Thus, binding to Nsl1 promotes a dramatic structural rearrangement in the core of RWD-N, which in turn promotes the repositioning of residues participating in Nsl1 binding.

Validation of the Knl1-Nsl1 Interaction

To assess the relevance of residues at the Knl1 interface with the Nsl1 peptide, we created the point mutants Knl1-Y2125G (Tyr to Gly) and Knl1-S2169E (Ser to Glu), as well as the double mutant Knl1-Y2125G-S2169E. All three Knl1 mutants were structurally stable (data not shown) but unable to interact with the $Nsl1^{258-281}$ synthetic peptide in ITC experiments (Figures 5A–5C). Conversely, a mutant $Nsl1^{258-281}$ peptide carrying the mutation Y270A (Tyr to Ala) was unable to interact with wild-type $Knl1^{2000-2311}$, validating the relevance of this residue for the high-affinity interaction of the Nsl1 C-terminal tail with Knl1 (Figure 5D).

Next, we generated inducible stable HeLa cell lines expressing wild-type $Knl1^{2107-2316}$ or the Y2125G and the S2169E mutants as an N-terminal fusion to GFP. All constructs expressed to similar levels upon induction of gene transcription with doxycycline (Figure 5E). In agreement with the biochemical experiments, the wild-type version of the Knl1 construct effectively pulled down endogenous Nsl1 from mitotically enriched cell extracts, but the Knl1-Y2125G and Knl1-S2169E mutants failed to do so (Figure 5E). Moreover, wild-type $Knl1^{2107-2316}$-GFP decorated kinetochores, while GFP fusions of mutant Knl1 did not show kinetochore recruitment (Figure 5F). Collectively, these experiments validate the Nsl1-binding interface identified by structural analysis and demonstrate that its interaction with Nsl1 is necessary for kinetochore recruitment of Knl1.

A 3D View of the KMN Network

To gain a more detailed understanding of the organization of the KMN network, we determined the 3D structure of Complex 4 (Mis12-C:$Knl1^{2106-2311}$:$Ndc80^{Bonsai}$) by negative-stain EM and single-particle analysis. The resulting map extended to a maximal resolution of 27 Å, as judged by Fourier shell correlation (Figure S2). The 3D maps of the engineered KMN network (Figure 6A) show an elongated structure with a long axis of ~35 nm, and a side element, 6–7 nm long, emerging approximately at half the height of the long axis with a defined 65° angle. We manually fitted the atomic coordinates of the $Ndc80^{Bonsai}$ (Ciferri et al., 2008) and of the Knl1 C-terminal domain as rigid bodies in the EM map of Complex 4. The crystallographic models of $Ndc80^{Bonsai}$ and $Knl1^{2091-2311}$ fitted well into the upper and lateral density, respectively (colored in gray and orange in Figure 6A), providing an unequivocal identification of their points of contact within the KMN assembly. As expected, the Spc24 and Spc25 moieties of Ndc80-C^{Bonsai} are located near the point of contact with Mis12-C. We attribute the remaining density (in

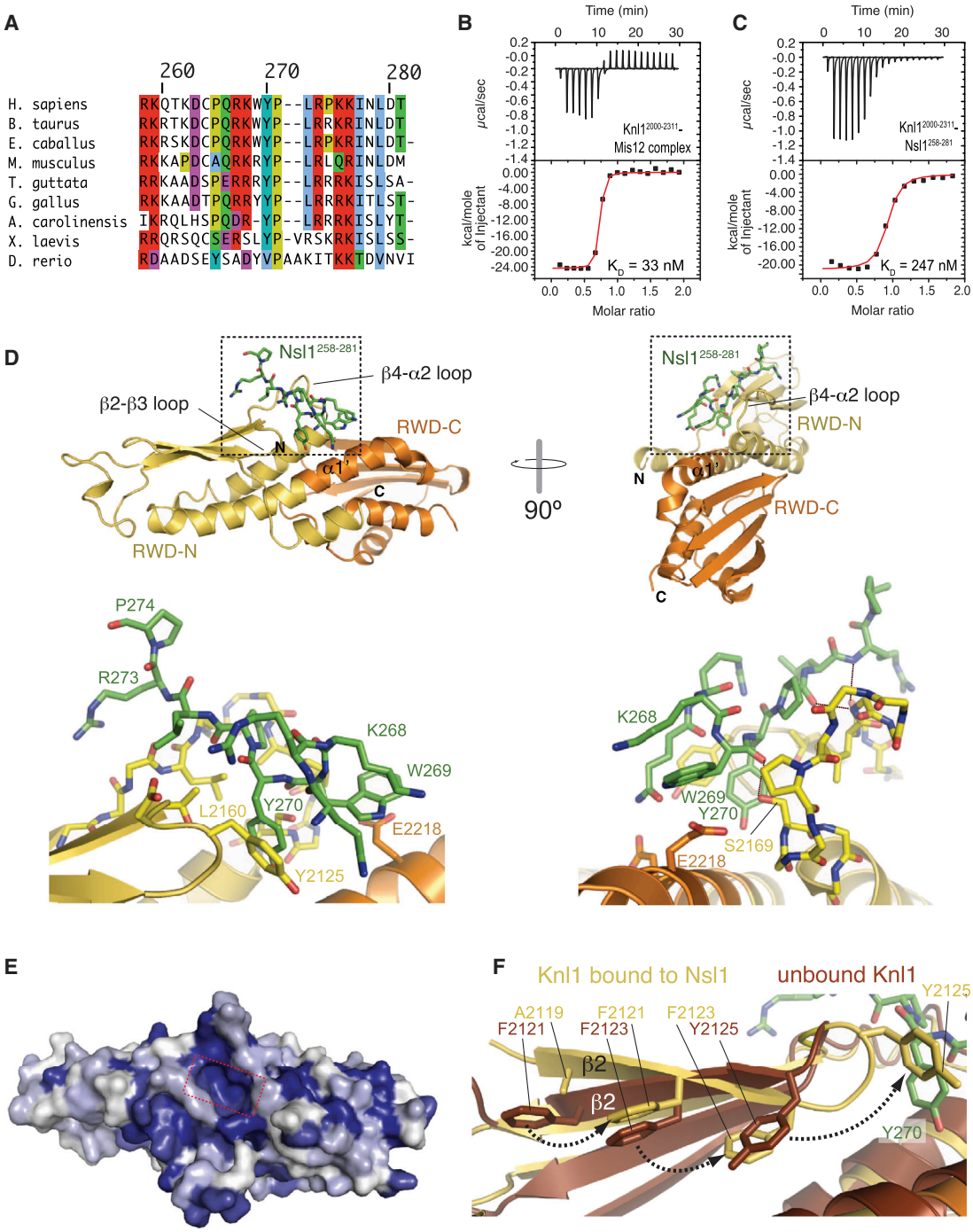

Figure 4. Biochemical and Structural Characterization of the Knl1-Nsl1 Complex

(A) Alignment of sequences of the C-terminal region of Nsl1 subunits in the indicated species. An alignment of a larger C-terminal segment of Nsl1 and containing additional orthologous sequences is shown in Figure S4.

(B) Characterization by ITC of the interaction of Knl1$^{2000\text{-}2311}$ with the Mis12 complex.

(C) Characterization by ITC of the interaction of Knl1$^{2000\text{-}2311}$ with a synthetic peptide encompassing residues 258–281 of Nsl1.

(D) Several views combining ball-and-stick and cartoon models of the complex of Knl1$^{2091\text{-}2311}$ with Nsl1$^{258\text{-}281}$.

(E) Conservation of residues in Knl1$^{2091\text{-}2311}$ was computed from an alignment of 13 Knl1 sequences (Figure S4) and mapped onto the surface of the Knl1 crystallographic model. The red rectangle marks the depression on which Y270^{Nsl1} inserts on Knl1.

(F) Cartoon and ball-and-stick model of the superimposed structures of the unbound (brown) and Nsl1-bound (yellow) Knl1 C-terminal domain depicting the conformational change in the hydrophobic core of RWD-N that leads to the extrusion of Y2125.

green) to the Mis12 complex. In agreement with the appearance of class averages in Figure 1, the base of the Mis12 "trunk," distal from the point of contact with the Knl1 and Ndc80 "branches," is distinctly thicker.

By using the F(ab) fragment of a monoclonal antibody directed against the N-terminal region of the Nsl1 subunit of the human Mis12-C (Figure S6), we mapped the N terminus of Nsl1 to the thick end of the Mis12 complex (Figure 6B). Conversely, gold labeling directed against the C-terminal hexahistidine tag of the Dsn1 subunit of MIS12-C positioned the metal label near the thin end where Ndc80 binding takes place (Figure 6C). This is consistent with the observation that this region of Dsn1 interacts with the Ndc80 complex (Malvezzi et al., 2013). Finally, we acquired images of negatively stained single particles of the Mis12-C:Knl1$^{2106-2316}$:Ndc80-C$^{full-length}$ complex (Figure 6D). In agreement with our previous analysis (Screpanti et al., 2011), it appeared elongated, ~75 nm in length, and structurally heterogeneous due to flexibility of the Ndc80 complex. Collectively, these results illuminate crucial structural and topological features of the KMN network.

DISCUSSION

The ability of the KMN network to coordinate tethering into chromatin, microtubule attachment, and mitotic checkpoint signaling is embedded in its structural organization. Structural analysis of the KMN network is therefore of great importance to develop a molecular understanding of kinetochore function. Our results shed new light on the structural organization of the KMN network. We report that the kinetochore-targeting C-terminal domain of Knl1 contains a tandem arrangement of RWD domains. Similarity in the topology of RWD-domain-containing kinetochore proteins (Figure 3) leads us to speculate that they diverged from an ancestor consisting of an N-terminal helical domain followed by one or two RWD domains. In kinetochore proteins, such arrangement is always dimeric. However, C-terminal fragments of Knl1 containing the majority of the predicted coiled-coil do not dimerize. We therefore speculate that Zwint satisfies the dimerization potential of the helical segment of Knl1. This hypothesis is consistent with the observation that Zwint is predicted to adopt an entirely helical conformation and contains two stretches with high propensity toward coiled-coil formation (Figure 1A). Thus, the Knl1-Zwint complex might be reminiscent of heterodimeric topologies of helical-RWD proteins such as Spc24 and Spc25, with the important difference that Zwint might have lost the RWD domain in the course of evolution. In agreement with a stabilizing role of Zwint on Knl1, depletion of Zwint leads to a reduction in the kinetochore levels of Knl1 (Varma et al., 2013).

Mis12-C acts as a receptor for the recruitment of the Spc24-Spc25 and Knl1-Zwint dimers, and in both cases the interaction is directed toward RWD domains in these target proteins. An exciting concept emerging from our observations is that Mis12-C is an intrinsically asymmetric protein, which docks to centromeric chromatin at one end, and that acts as a multivalent receptor for RWD-containing proteins at the other end. The Nsl1 subunit of Mis12-C plays a crucial role in this process. It provides a docking site for the Spc24-Spc25 dimer, centered at a Pro-Val-Ile-His-Leu motif encompassing residues 209–213 (Petrovic et al., 2010), as well as a docking site for the Knl1 RWD domains, approximately 60 residues toward the C terminus, and centered around residue Tyr270^{Nsl1}. At least in *Saccharomyces cerevisiae*, the C-terminal tail of Dsn1 has been shown to provide a second docking site for the Spc24-Spc25 complex (Malvezzi et al., 2013).

How far-reaching is the view that Mis12-C is an interaction hub for RWD-containing proteins? The Mis12 complex of *Saccharomyces cerevisiae* (known as MIND or Mtw1 complex in this organism) has been implicated in the recruitment of the four-subunit monopolin complex, which is essential for kinetochore coorientation during the first meiotic division of *Saccharomyces cerevisiae* (Tóth et al., 2000). Interestingly, the RWD domain of the monopolin subunit Csm1 (Figure 3A) interacts with a motif in the N-terminal region of the Dsn1 subunit of Mis12-C (Corbett et al., 2010; Sarkar et al., 2013) (Figure 6D). The *S. cerevisiae* COMA complex, consisting of the four subunits Ame1, Okp1, Ctf19, and Mcm21 (respectively related to Cenp-Q, Cenp-U, Cenp-O, and Cenp-P), the latter two of which contain RWD domains, also binds directly to the Mis12 complex (Hornung et al., 2011). It is unclear, however, whether the RWD domains of Ctf19 and Mcm21 are directly involved in this interaction and what part of the yeast Mis12-C is involved (Figure 6D). Also unclear is whether these two additional examples of Mis12-C:RWD interactions are conserved in other organisms. Finally, it is unknown whether the Mad1 RWD domain interacts directly with the Mis12 complex. Nevertheless, when taken collectively these observations strongly reinforce the idea that the subunits of Mis12-C have specialized in the interaction with RWD domains. At present, there is insufficient structural information on the interactions of RWD domains with Mis12-C motifs to be able to draw any conclusion on the generality of the binding mechanisms involved, except that RWD modules appear to have a preference for N- or C-terminal flexible parts of the Mis12-C subunits.

Another important development brought about by our studies is the availability of the first 3D structure of a KMN network complex. Previously, 2D negative-stain EM analyses provided insight into the overall shape of the Ndc80 and Mis12 complexes (Gonen et al., 2012; Hornung et al., 2011; Maskell et al., 2010; Petrovic et al., 2010; Screpanti et al., 2011; Wang et al., 2008; Wei et al., 2005), while hybrid methods have shed light on the interaction of the Ndc80 complex with microtubules (Alushin et al., 2012, 2010). By fitting the crystal structures of the Ndc80-C^{Bonsai} complex (Ciferri et al., 2008) and of C-terminal region of Knl1 (this study) into the 3D structure of Complex 4, we unequivocally identify the relative position of the RWD-containing subunits that interact with the Mis12 complex.

Our studies also impose significant restraints on the organization of the Nsl1 subunit within the Mis12 complex. By combining antibody labeling with EM, we determined that the N-terminal region of Nsl1 is positioned near the thick end of Mis12-C. Because Spc24 and Spc25 bind at the opposite end of Mis12-C and interact there with the PVIHL motif at residues 209–213 of Nsl1, our data imply that the first 210 residues of the Nsl1 chain extend longitudinally along the entire length of the Mis12 complex (approximately 20 nm), at which point the Nsl1 chain bends to reach the Nsl1-binding interface of the RWD domains of Knl1,

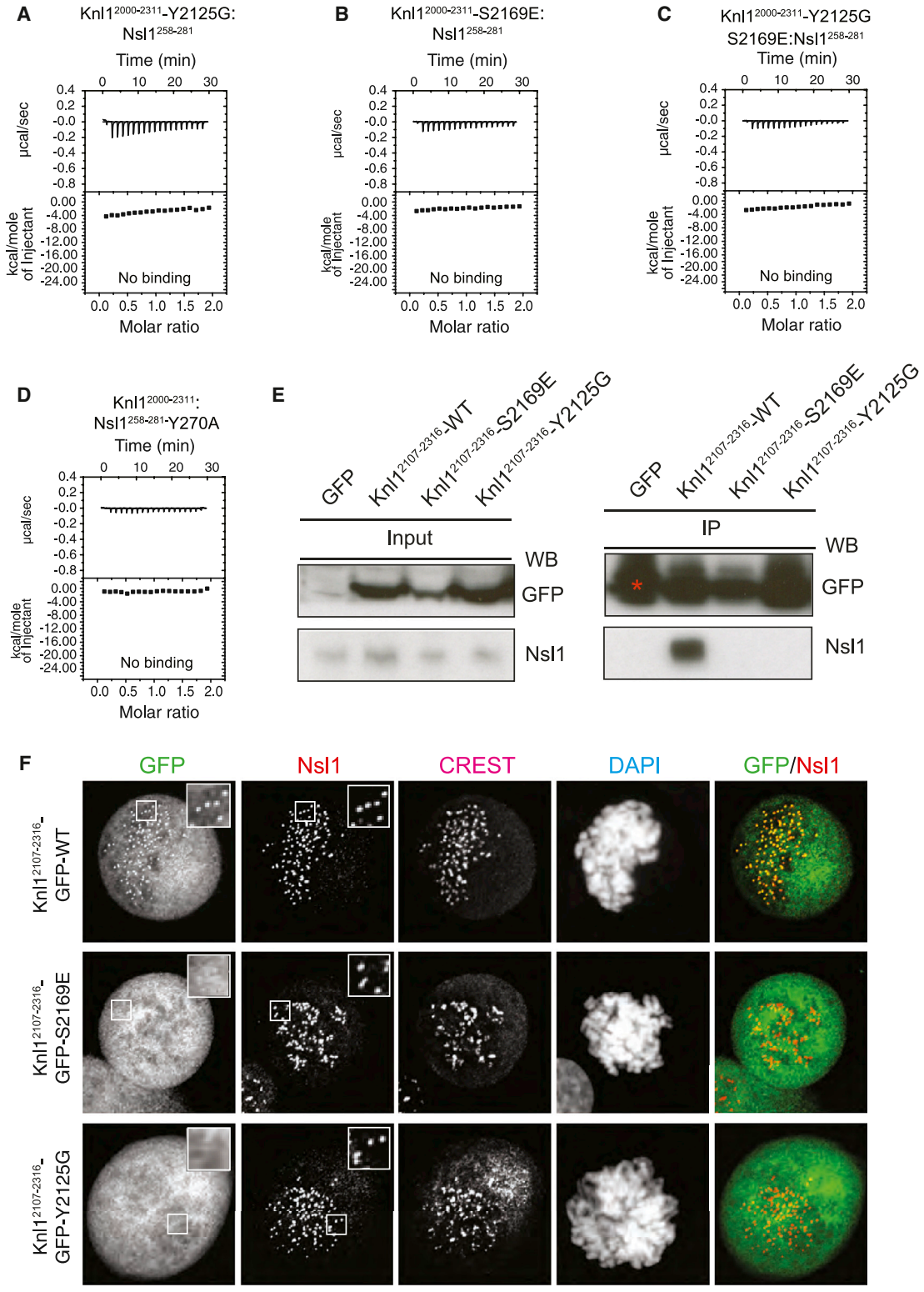

Figure 5. Validation of the Knl1-Nsl1 Interaction Mechanism

(A–C) ITC analysis of the interaction of the indicated Knl1$^{2000-2311}$ mutant constructs with the Nsl1$^{258-281}$ synthetic peptide. The thermogram of the interaction of wild-type Knl1$^{2000-2311}$ with Nsl1$^{258-281}$ is shown in Figure 4C.

(D) ITC analysis of the interaction of wild-type Knl1$^{2000-2311}$ with a mutant version of the Nsl1$^{258-281}$ peptide carrying the Tyr270 to Ala mutation.

(legend continued on next page)

approximately 3 nm away from the central axis of the Mis12 density (Figure 6D).

The 3D analysis of the KMN network provides an exceptionally faithful framework to rationalize the results of a superresolution light-microscopy approach designed to identify the relative coordinates of KMN subunits along the interkinetochore axis in human or marsupial cells (Dumont et al., 2012; Varma et al., 2013; Wan et al., 2009). In the superresolution analysis, whose results are summarized in Figure 6E, the Knl1 N-terminal region was shown to be positioned approximately 20 nm above (i.e., in the direction of the microtubule in Figure 6E) the Spc24 and Spc25 subunits or the C-terminal region of Zwint. We speculate that this position might be defined by the length and orientation of the predicted helical segment of the Knl1-Zwint dimer, as well as by the specific mechanism of dimerization mediated by the N-terminal region of Knl1. Our future studies will aim to unravel the mechanism of dimerization, an effort that has so far been thwarted by poor solubility of the suitable recombinant constructs.

The region between the N-terminal dimerization motif and the predicted helical segment of Knl1 is enriched in motifs that mediate the recruitment of checkpoint proteins. Most notably, these include the Met-Glu-Leu-Thr (MELT) motifs, which are present in multiple copies along the sequence of Knl1, and which mediate the recruitment of the checkpoint protein Bub3, of its binding partners Bub1 and BubR1, and of downstream checkpoint components (London et al., 2012; Primorac et al., 2013; Shepperd et al., 2012; Yamagishi et al., 2012). This region of Knl1 might form a layer, at an intermediate distance between the microtubule-binding interface of the kinetochore and the Mis12 hub, where checkpoint signaling takes place. Consistently, the superresolution analysis identified the checkpoint proteins at this height of the interkinetochore axis (Varma et al., 2013; Wan et al., 2009).

In conclusion, the biochemical reconstitution and structural analysis of KMN particles discussed here contributes to a deeper understanding of crucial interactions at kinetochores, thus providing ever more accurate ways to manipulate kinetochores for functional purposes.

EXPERIMENTAL PROCEDURES

Plasmids

The cDNA sequence encoding KNL1$^{2107-2316}$-GFP (wild-type) was amplified by PCR from a pEGFP-C1 vector containing *KNL1* full-length sequence (isoform 2; gift from Prof. M. Yanagida, University of Kyoto) and subcloned into the pcDNA5/FRT/TO-IRES vector (a derivative of the pcDNA 5/FRT/TO plasmid, Invitrogen). Site-directed mutagenesis, performed with QuikChange Mutagenesis Lit (Agilent Technologies), was used to generate mutant versions of the plasmid. The pcDNA 5/FRT/TO-GFP vector was obtained by subcloning the sequence encoding eGFP from pEGFP-C1 (Clontech) into the pcDNA 5/FRT/TO-IRES vector. Plasmids were verified by DNA sequencing. The Knl1$^{1-250+2107-2316}$-GFP fusion was generated using a PCR based cloning strategy (see the Supplemental Experimental Procedures). For recombinant protein expression, sequences encoding C-terminal Knl1 fragments (Knl1$^{2000-2311}$, Knl1$^{2091-2311}$, Knl1$^{2106-2311}$) were subcloned in pGEX-6P-2rbs, a dicistronic derivative of pGEX6P, generated in house. Sequences encoding variant versions of Mis12 complex were generated using standard restriction-based cloning procedures. Site-directed mutagenesis required to generate mutant versions of expression vectors was performed with QuikChange Mutagenesis Kit (Agilent Technologies).

Cell Culture

Flp-In T-Rex HeLa cell lines were generated and maintained as described in Supplemental Experimental Procedures section. Transgene expression was induced by the addition of 20–50 ng/ml Doxycycline (Sigma) for 24 hr. Nocodazole (Sigma) was used at a concentration of 80 ng/mL for 16 hr.

Protein Expression and Purification

We used a truncated variant of the Mis12 complex (Mis12^{Nano}) lacking segments susceptible to limited proteolysis and not involved in the interaction with Ndc80 or Knl1 (full-length Mis12, Nnf1$^{31-205}$, Nsl1$^{1-206}$, Dsn1$^{68-356}$). *E. coli* BL21(DE3)-Codon-plus-RIL cells containing the pST39 plasmid encoding Mis12^{Nano} were grown in Terrific broth at 37°C to an OD_{600} of ≈0.8. Protein expression was induced by the addition of 0.1 mM IPTG at 18°C, and cells were incubated overnight. Cell pellets were resuspended (for buffer composition, see Supplemental Experimental Procedures), lysed by sonication, and cleared by centrifugation. The cleared lysate was purified through a succession of Ni-NTA (QIAGEN), ResourceQ, and Superdex 200 10/300 column (GE Healthcare). Coexpression of Mis12^{Nanoextra} variant (full-length Mis12, Nnf1$^{31-205}$, full-length Nsl1, Dns1$^{68-356}$) with the Knl1$^{2106-2316}$ fragment was carried out as described in Supplemental Experimental Procedures.

Crystallization and Data Collection

Knl1$^{2106-2311}$ was crystallized at approximately 6.6 mg/ml, in sitting drops in 96-well plates set up with a Honeybee Cartesian robot. Optimization of initial hits was performed manually using a hanging-drop procedure in 24-well plates (5–7 mg/ml at 20°C) containing a 1:1 mixture of protein and precipitant solution (120–300 KSCN, 100 mM BisTris Propane [pH 8.6–9.2], 17% [v/v] PEG 3350 and 1 mM DTT). X-ray diffraction of a native crystal to 2.5 Å was collected at beamline ID14-1 of the European Synchrotron Radiation Facility (ESRF, France). Heavy atom derivatives were prepared by soaking native crystals in 10 mM K_2PtBr_4 for 16 hr or 500 mM NaBr (25"). Crystals of the Knl1:Nsl1 peptide complex diffracted to a maximum resolution of 2.8 Å at PXIII beamline of the Swiss Light Source (SLS, Switzerland). Structure determination was performed as described in Supplemental Experimental Procedures.

Electron Microscopy and Image Analysis

Of the protein sample, 4 μl was adsorbed onto glow-discharged carbon-coated grids prior to negative staining with uranyl formate (SPI Supplies/Structure Probe). Samples were imaged with a JEOL1400 microscope equipped with a LaB_6 cathode operated at 120 kV. Images were recorded at low-dose conditions at a magnification of 67,200× on a 4,000 × 4,000 CCD camera F416 (TVIPS). Data analysis and further processing are described in Supplemental Experimental Procedures.

Additional Methods

Production of monoclonal antibodies is described in Supplemental Experimental Procedures. Fab fragments were generated by digestion with immobilized papain (Pierce) and further purification as described in Supplemental

(E) Interaction analysis of the indicated Knl1$^{2107-2316}$-GFP constructs that were expressed in HeLa Flp-In T-REx cells (Tighe et al., 2008) from stably integrated transgenes after induction with doxycycline. Immunoprecipitations (IP) were carried out using an anti-GFP antibody. Detection of candidate proteins was performed by western blot analysis. Mis12-C subunit Nsl1 was identified only in precipitates of wild-type Knl1-GFP construct but not of mutant constructs. The asterisk indicates an unspecific band.

(F) Localization analysis of wild-type and mutant Knl1 C-terminal domain in the HeLa cell lines discussed in (E). Colocalization of the GFP signal with the kinetochore markers Nsl1 and CREST indicated kinetochore localization. Kinetochore localization is evident for the wild-type Knl1 construct, but not for the mutant constructs.

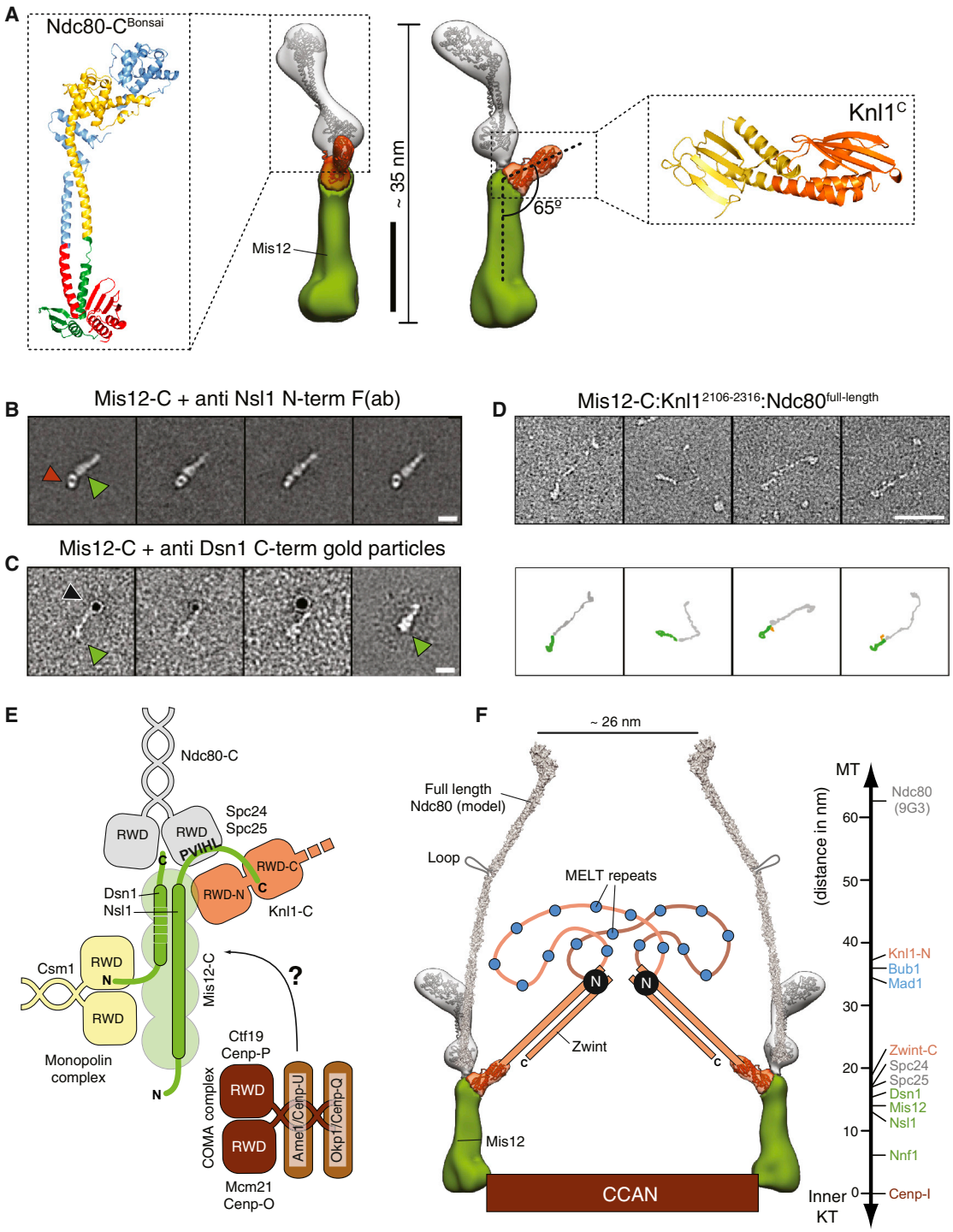

Figure 6. 3D EM Structure of Complex 4 and a Model of the KMN Network

(A) A 3D reconstruction of Complex 4 (see Figure 1G) from negatively stained particles. Available high-resolution experimental structures of KMN fragments were fitted into the density. The long axis is approximately 35 nm. The lateral density attributed to the Knl1 C-terminal domain emerges at a 65° angle from the long axis. Scale bar, 10 nm.

(B) Representative class averages of negatively stained EM images of Mis12-C (green arrowhead) bound to the F(ab) of a monoclonal antibody directed against the N-terminal region of Nsl1 (red arrowhead; see Figure S6). Scale bar, 10 nm.

(C) Single Mis12 complexes (left, green arrowhead) labeled with Ni-NTA-nano-gold directed against the C-terminal region of Dsn1 (black arrowhead; see Figure S6) in comparison to a representative class average of Mis12-C (right). Scale bar, 10 nm.

(legend continued on next page)

Experimental Procedures. ITC was performed on an ITC200 microcalorimeter (GE Healthcare). Data were fitted by least-square procedure to a single-site binding model using ORIGIN software package (MicroCal). More details on the procedure are presented in Supplemental Experimental Procedures. Methods describing experiments of fluorescence microscopy, immunoprecipitation, and western blotting are described in detail in Supplemental Experimental Procedures.

ACCESSION NUMBERS

The final models and the structure factor amplitudes have been submitted to the Protein Data Bank under the accession numbers 4NFA (unliganded Knl1) and 4NF9 (Knl1:Nsl1 complex). The EM map has been deposited in the EM Data Bank under the accession code EMD-2549.

SUPPLEMENTAL INFORMATION

Supplemental Information includes six figures and Supplemental Experimental Procedures and can be found with this article at http://dx.doi.org/10.1016/j.molcel.2014.01.019.

AUTHOR CONTRIBUTIONS

A.P. prepared samples for EM analysis, and S.M. collected and processed EM data (under the supervision of S.R.). A.P., J.K., V.C., and S.P. carried out crystallization and X-ray crystallography analyses of Knl1 and Knl1-Nsl1 complexes. A.P., M.M., K.O., and V.K. conceived of and executed biochemical and immunofluorescence experiments in HeLa cells. A.D.A. contributed to preparing and characterizing antibodies against the Mis12 complex. A.P. and S.W. carried out experiments of protein expression, purification, and biochemical characterization. A.P., S.M., J.K., S.R., and A.M. prepared figures and tables. A.M. coordinated the team, and wrote and revised the paper.

ACKNOWLEDGMENTS

We are grateful to members of the Musacchio laboratory for helpful discussions. We thank Ingrid Vetter, Marco Bürger, and the staff of the European Synchroton Radiation Facility (ESRF) and of the Swiss Light Source (SLS) for precious help in X-ray diffraction data collection; Silvia Monzani for preparations of the Mis12 complex; Oliver Hofnagel for assistance at the electron microscope; Nicoletta Caridi, Mario Cinquanta, Giseppe Ossolengo, and Marisa Aliprandi for the generation of monoclonal antibodies; and Fabrizio Villa, Siva Jeganathan, and Marion Pesenti for help with different aspects of the project. A.M. acknowledges funding by the European Union's 7th Framework Program ERC agreement KINCON and the Integrated Project MitoSys. S.R. is supported by the "Deutsche Forschungsgemeinschaft" Grant RA 1781/1-1.

Received: November 12, 2013
Revised: December 26, 2013
Accepted: January 9, 2014
Published: February 13, 2014

REFERENCES

Alushin, G.M., Ramey, V.H., Pasqualato, S., Ball, D.A., Grigorieff, N., Musacchio, A., and Nogales, E. (2010). The Ndc80 kinetochore complex forms oligomeric arrays along microtubules. Nature *467*, 805–810.

Alushin, G.M., Musinipally, V., Matson, D., Tooley, J., Stukenberg, P.T., and Nogales, E. (2012). Multimodal microtubule binding by the Ndc80 kinetochore complex. Nat. Struct. Mol. Biol. *19*, 1161–1167.

Bock, L.J., Pagliuca, C., Kobayashi, N., Grove, R.A., Oku, Y., Shrestha, K., Alfieri, C., Golfieri, C., Oldani, A., Dal Maschio, M., et al. (2012). Cnn1 inhibits the interactions between the KMN complexes of the yeast kinetochore. Nat. Cell Biol. *14*, 614–624.

Burroughs, A.M., Jaffee, M., Iyer, L.M., and Aravind, L. (2008). Anatomy of the E2 ligase fold: implications for enzymology and evolution of ubiquitin/Ub-like protein conjugation. J. Struct. Biol. *162*, 205–218.

Cheeseman, I.M., and Desai, A. (2008). Molecular architecture of the kinetochore-microtubule interface. Nat. Rev. Mol. Cell Biol. *9*, 33–46.

Cheeseman, I.M., Chappie, J.S., Wilson-Kubalek, E.M., and Desai, A. (2006). The conserved KMN network constitutes the core microtubule-binding site of the kinetochore. Cell *127*, 983–997.

Ciferri, C., De Luca, J., Monzani, S., Ferrari, K.J., Ristic, D., Wyman, C., Stark, H., Kilmartin, J., Salmon, E.D., and Musacchio, A. (2005). Architecture of the human ndc80-hec1 complex, a critical constituent of the outer kinetochore. J. Biol. Chem. *280*, 29088–29095.

Ciferri, C., Pasqualato, S., Screpanti, E., Varetti, G., Santaguida, S., Dos Reis, G., Maiolica, A., Polka, J., De Luca, J.G., De Wulf, P., et al. (2008). Implications for kinetochore-microtubule attachment from the structure of an engineered Ndc80 complex. Cell *133*, 427–439.

Corbett, K.D., Yip, C.K., Ee, L.-S., Walz, T., Amon, A., and Harrison, S.C. (2010). The monopolin complex crosslinks kinetochore components to regulate chromosome-microtubule attachments. Cell *142*, 556–567.

DeLuca, J.G., Gall, W.E., Ciferri, C., Cimini, D., Musacchio, A., and Salmon, E.D. (2006). Kinetochore microtubule dynamics and attachment stability are regulated by Hec1. Cell *127*, 969–982.

(D) (Upper panel) Negatively stained single particles of the Mis12-C:Knl1$^{2106-2311}$:Ndc80-C$^{full-length}$ complex. (Lower panel) Traces interpreting the density of the complex in terms of its components. Scale bar, 50 nm.
(E) A summary of interactions and topological relationships within the KMN network. The Nsl1 subunit of Mis12-C extends along the length of the entire complex, interacting with Spc24-Spc25 at residues 209–213, and with Knl1 around residues 266–274. The C-terminal region of Dsn1 has also been shown to bind Spc24-Spc25 (Malvezzi et al., 2013). RWD domains from different proteins, shown as squares with rounded corners, decorate the Mis12 complex. The position of the N-terminal tail of Dsn1 is unknown, but prediction methods indicate that Dsn1 is also extended. In *S. cerevisiae*, an N-terminal extension of Dsn1, not present in other orthologs, is responsible for the interaction with Csm1. How the COMA complex binds Mis12-C is also unclear.
(F) A model of kinetochore organization. The model incorporates the 3D structure of the KMN network shown in (A). A previously published model of the full-length Ndc80 complex (Ciferri et al., 2008) is shown, with its Spc24-Spc25 heads superimposed on that of the Ndc80-C^{Bonsai} complex fitted into the 3D map. An insertion in the predicted coiled-coil region of the Ndc80 subunit expected to create a gap in the coiled-coil (Ciferri et al., 2008) is indicated by a loop. The vertical line on the right indicates the inter-kinetochore axis. The position of the indicated proteins along this axis reports the distance of the centroid of the fluorescence distribution of each of the indicated proteins (labeled with a fluorescence tag or by fluorescent antibodies) from a common reference signal (in this case, the CCAN subunit CENP-I, taken to represent the zero value) in human cells at metaphase (Varma et al., 2013; Wan et al., 2009). The vertical alignment of the 3D model to this scale was based on the predicted position of Nnf1 at the bottom of the Mis12 complex (Maskell et al., 2010; Petrovic et al., 2010) and by the constrain that Complex 4 is approximately 35 nm. Note that the epitope recognized by the anti-Ndc80 (Hec1) antibody 9G3 has been mapped to residues 200–215 of Ndc80 (DeLuca et al., 2006). The depicted mechanism of Knl1 dimerization by the Knl1 N-terminal domain is fictional. The region comprised between the N terminus of Knl1 and its predicted coiled-coil domain is predicted disordered. The function of MELT repeats in this region as a docking basis for checkpoint proteins (London et al., 2012; Primorac et al., 2013; Shepperd et al., 2012; Yamagishi et al., 2012) might explain the observed position of checkpoint proteins along the interkinetochore axis (Varma et al., 2013). MT, microtubule; KT, kinetochore.

Doerks, T., Copley, R.R., Schultz, J., Ponting, C.P., and Bork, P. (2002). Systematic identification of novel protein domain families associated with nuclear functions. Genome Res. *12*, 47–56.

Dumont, S., Salmon, E.D., and Mitchison, T.J. (2012). Deformations within moving kinetochores reveal different sites of active and passive force generation. Science *337*, 355–358.

Espeut, J., Cheerambathur, D.K., Krenning, L., Oegema, K., and Desai, A. (2012). Microtubule binding by KNL-1 contributes to spindle checkpoint silencing at the kinetochore. J. Cell Biol. *196*, 469–482.

Foley, E.A., and Kapoor, T.M. (2013). Microtubule attachment and spindle assembly checkpoint signalling at the kinetochore. Nat. Rev. Mol. Cell Biol. *14*, 25–37.

Gascoigne, K.E., Takeuchi, K., Suzuki, A., Hori, T., Fukagawa, T., and Cheeseman, I.M. (2011). Induced ectopic kinetochore assembly bypasses the requirement for CENP-A nucleosomes. Cell *145*, 410–422.

Gonen, S., Akiyoshi, B., Iadanza, M.G., Shi, D., Duggan, N., Biggins, S., and Gonen, T. (2012). The structure of purified kinetochores reveals multiple microtubule-attachment sites. Nat. Struct. Mol. Biol. *19*, 925–929.

Hodson, C., Cole, A.R., Lewis, L.P.C., Miles, J.A., Purkiss, A., and Walden, H. (2011). Structural analysis of human FANCL, the E3 ligase in the Fanconi anemia pathway. J. Biol. Chem. *286*, 32628–32637.

Hori, T., Amano, M., Suzuki, A., Backer, C.B., Welburn, J.P., Dong, Y., McEwen, B.F., Shang, W.-H., Suzuki, E., Okawa, K., et al. (2008). CCAN makes multiple contacts with centromeric DNA to provide distinct pathways to the outer kinetochore. Cell *135*, 1039–1052.

Hornung, P., Maier, M., Alushin, G.M., Lander, G.C., Nogales, E., and Westermann, S. (2011). Molecular architecture and connectivity of the budding yeast Mtw1 kinetochore complex. J. Mol. Biol. *405*, 548–559.

Joglekar, A.P., Bouck, D.C., Molk, J.N., Bloom, K.S., and Salmon, E.D. (2006). Molecular architecture of a kinetochore-microtubule attachment site. Nat. Cell Biol. *8*, 581–585.

Joglekar, A.P., Bloom, K., and Salmon, E.D. (2009). In vivo protein architecture of the eukaryotic kinetochore with nanometer scale accuracy. Curr. Biol. *19*, 694–699.

Johnston, K., Joglekar, A., Hori, T., Suzuki, A., Fukagawa, T., and Salmon, E.D. (2010). Vertebrate kinetochore protein architecture: protein copy number. J. Cell Biol. *189*, 937–943.

Kim, S., Sun, H., Tomchick, D.R., Yu, H., and Luo, X. (2012). Structure of human Mad1 C-terminal domain reveals its involvement in kinetochore targeting. Proc. Natl. Acad. Sci. USA *109*, 6549–6554.

Kiyomitsu, T., Obuse, C., and Yanagida, M. (2007). Human Blinkin/AF15q14 is required for chromosome alignment and the mitotic checkpoint through direct interaction with Bub1 and BubR1. Dev. Cell *13*, 663–676.

Kiyomitsu, T., Iwasaki, O., Obuse, C., and Yanagida, M. (2010). Inner centromere formation requires hMis14, a trident kinetochore protein that specifically recruits HP1 to human chromosomes. J. Cell Biol. *188*, 791–807.

Kiyomitsu, T., Murakami, H., and Yanagida, M. (2011). Protein interaction domain mapping of human kinetochore protein Blinkin reveals a consensus motif for binding of spindle assembly checkpoint proteins Bub1 and BubR1. Mol. Cell. Biol. *31*, 998–1011.

Kline, S.L., Cheeseman, I.M., Hori, T., Fukagawa, T., and Desai, A. (2006). The human Mis12 complex is required for kinetochore assembly and proper chromosome segregation. J. Cell Biol. *173*, 9–17.

Krenn, V., Wehenkel, A., Li, X., Santaguida, S., and Musacchio, A. (2012). Structural analysis reveals features of the spindle checkpoint kinase Bub1-kinetochore subunit Knl1 interaction. J. Cell Biol. *196*, 451–467.

Krenn, V., Overlack, K., Primorac, I., van Gerwen, S., and Musacchio, A. (2014). KI motifs of human Knl1 enhance assembly of comprehensive spindle checkpoint complexes around MELT repeats. Curr. Biol. *24*, 29–39.

Lara-Gonzalez, P., Westhorpe, F.G., and Taylor, S.S. (2012). The spindle assembly checkpoint. Curr. Biol. *22*, R966–R980.

Liu, D., Vleugel, M., Backer, C.B., Hori, T., Fukagawa, T., Cheeseman, I.M., and Lampson, M.A. (2010). Regulated targeting of protein phosphatase 1 to the outer kinetochore by KNL1 opposes Aurora B kinase. J. Cell Biol. *188*, 809–820.

London, N., Ceto, S., Ranish, J.A., and Biggins, S. (2012). Phosphoregulation of Spc105 by Mps1 and PP1 regulates Bub1 localization to kinetochores. Curr. Biol. *22*, 900–906.

Malvezzi, F., Litos, G., Schleiffer, A., Heuck, A., Mechtler, K., Clausen, T., and Westermann, S. (2013). A structural basis for kinetochore recruitment of the Ndc80 complex via two distinct centromere receptors. EMBO J. *32*, 409–423.

Maskell, D.P., Hu, X.-W., and Singleton, M.R. (2010). Molecular architecture and assembly of the yeast kinetochore MIND complex. J. Cell Biol. *190*, 823–834.

Meadows, J.C., Shepperd, L.A., Vanoosthuyse, V., Lancaster, T.C., Sochaj, A.M., Buttrick, G.J., Hardwick, K.G., and Millar, J.B.A. (2011). Spindle checkpoint silencing requires association of PP1 to both Spc7 and kinesin-8 motors. Dev. Cell *20*, 739–750.

Nishino, T., Rago, F., Hori, T., Tomii, K., Cheeseman, I.M., and Fukagawa, T. (2013). CENP-T provides a structural platform for outer kinetochore assembly. EMBO J. *32*, 424–436.

Pagliuca, C., Draviam, V.M., Marco, E., Sorger, P.K., and De Wulf, P. (2009). Roles for the conserved spc105p/kre28p complex in kinetochore-microtubule binding and the spindle assembly checkpoint. PLoS ONE *4*, e7640.

Petrovic, A., Pasqualato, S., Dube, P., Krenn, V., Santaguida, S., Cittaro, D., Monzani, S., Massimiliano, L., Keller, J., Tarricone, A., et al. (2010). The MIS12 complex is a protein interaction hub for outer kinetochore assembly. J. Cell Biol. *190*, 835–852.

Primorac, I., Weir, J.R., Chiroli, E., Gross, F., Hoffmann, I., van Gerwen, S., Ciliberto, A., and Musacchio, A. (2013). Bub3 reads phosphorylated MELT repeats to promote spindle assembly checkpoint signaling. eLife *2*, e01030–e01030.

Przewloka, M.R., Venkei, Z., Bolanos-Garcia, V.M., Debski, J., Dadlez, M., and Glover, D.M. (2011). CENP-C is a structural platform for kinetochore assembly. Curr. Biol. *21*, 399–405.

Rosenberg, J.S., Cross, F.R., and Funabiki, H. (2011). KNL1/Spc105 recruits PP1 to silence the spindle assembly checkpoint. Curr. Biol. *21*, 942–947.

Santaguida, S., and Musacchio, A. (2009). The life and miracles of kinetochores. EMBO J. *28*, 2511–2531.

Sarkar, S., Shenoy, R.T., Dalgaard, J.Z., Newnham, L., Hoffmann, E., Millar, J.B.A., and Arumugam, P. (2013). Monopolin subunit Csm1 associates with MIND complex to establish monopolar attachment of sister kinetochores at meiosis I. PLoS Genet. *9*, e1003610.

Schleiffer, A., Maier, M., Litos, G., Lampert, F., Hornung, P., Mechtler, K., and Westermann, S. (2012). CENP-T proteins are conserved centromere receptors of the Ndc80 complex. Nat. Cell Biol. *14*, 604–613.

Schmitzberger, F., and Harrison, S.C. (2012). RWD domain: a recurring module in kinetochore architecture shown by a Ctf19-Mcm21 complex structure. EMBO Rep. *13*, 216–222.

Screpanti, E., De Antoni, A., Alushin, G.M., Petrovic, A., Melis, T., Nogales, E., and Musacchio, A. (2011). Direct binding of Cenp-C to the Mis12 complex joins the inner and outer kinetochore. Curr. Biol. *21*, 391–398.

Shepperd, L.A.L., Meadows, J.C.J., Sochaj, A.M.A., Lancaster, T.C.T., Zou, J.J., Buttrick, G.J.G., Rappsilber, J.J., Hardwick, K.G.K., and Millar, J.B.A.J. (2012). Phosphodependent recruitment of Bub1 and Bub3 to Spc7/KNL1 by Mph1 kinase maintains the spindle checkpoint. Curr. Biol. *22*, 891–899.

Tighe, A., Staples, O., and Taylor, S. (2008). Mps1 kinase activity restrains anaphase during an unperturbed mitosis and targets Mad2 to kinetochores. J. Cell Biol. *181*, 893–901.

Tóth, A., Rabitsch, K.P., Gálová, M., Schleiffer, A., Buonomo, S.B., and Nasmyth, K. (2000). Functional genomics identifies monopolin: a kinetochore protein required for segregation of homologs during meiosis i. Cell *103*, 1155–1168.

Varma, D., Wan, X., Cheerambathur, D., Gassmann, R., Suzuki, A., Lawrimore, J., Desai, A., and Salmon, E.D. (2013). Spindle assembly checkpoint proteins are positioned close to core microtubule attachment sites at kinetochores. J. Cell Biol. *202*, 735–746.

Wan, X., O'Quinn, R.P., Pierce, H.L., Joglekar, A.P., Gall, W.E., DeLuca, J.G., Carroll, C.W., Liu, S.T., Yen, T.J., McEwen, B.F., et al. (2009). Protein architecture of the human kinetochore microtubule attachment site. Cell *137*, 672–684.

Wang, H.-W., Long, S., Ciferri, C., Westermann, S., Drubin, D., Barnes, G., and Nogales, E. (2008). Architecture and flexibility of the yeast Ndc80 kinetochore complex. J. Mol. Biol. *383*, 894–903.

Wei, R.R., Sorger, P.K., and Harrison, S.C. (2005). Molecular organization of the Ndc80 complex, an essential kinetochore component. Proc. Natl. Acad. Sci. USA *102*, 5363–5367.

Wei, R.R., Schnell, J.R., Larsen, N.A., Sorger, P.K., Chou, J.J., and Harrison, S.C. (2006). Structure of a central component of the yeast kinetochore: the Spc24p/Spc25p globular domain. Structure *14*, 1003–1009.

Wei, R.R., Al-Bassam, J., and Harrison, S.C. (2007). The Ndc80/HEC1 complex is a contact point for kinetochore-microtubule attachment. Nat. Struct. Mol. Biol. *14*, 54–59.

Westermann, S., and Schleiffer, A. (2013). Family matters: structural and functional conservation of centromere-associated proteins from yeast to humans. Trends Cell Biol. *23*, 260–269.

Yamagishi, Y., Yang, C.-H., Tanno, Y., and Watanabe, Y. (2012). MPS1/Mph1 phosphorylates the kinetochore protein KNL1/Spc7 to recruit SAC components. Nat. Cell Biol. *14*, 746–752.